Quantum Electronics **48** (3) 235–243 (2018) ©2018 Kvantovaya Elektronika and Turpion Ltd

INTERACTION OF LASER RADIATION WITH MATTER https://doi.org/10.1070/QEL16590

Processes of interaction of laser radiation with porous transparent materials during their ablation

V.V. Osipov, V.V. Lisenkov, V.V. Platonov, E.V. Tikhonov

Abstract. **The effect of ytterbium fibre laser radiation with λ = 1.07 μm on the pressed micropowders of transparent oxides and fluorides (CaF_2, Y_2O_3, Al_2O_3, YSZ, etc.) having low absorption coefficients is theoretically studied. Using the numerical modelling, it is established that the radiation scattering in the medium of particles 0.5–4.6 μm in diameter leads to the concentration of radiation in the local regions of the medium, with the intensity level exceeding the intensity of the incident radiation (0.46 MW cm^{-2}) by many times. It is shown that with the growth of the refractive index n of the material from 1.38 (MgF_2) to 2.12 (YSZ) the intensity of radiation in the region of the strongest local maximum increases from 3.8 to 31 MW cm^{-2}. In our opinion, this factor can be dominant in determining the possibility of achieving the ablation of such a medium by means of the radiation having an intensity of no greater than 1 MW cm^{-2}. This hypothesis is experimentally checked by the example of preparing a nanopowder of CaF_2 (n = 1.43) and 1% Nd:Y_2O_3 (n = 1.91) by evaporating the pressed target with the porosity 50% by the continuous-wave radiation of the ytterbium fibre laser with the power 600 W and the intensity 0.4 MW cm^{-2}. Inside the CaF_2 target, the scattered radiation intensity is smaller than the optical breakdown threshold, and the target is not evaporated. Under the same conditions, the target made of higher-melting 1% Nd:Y_2O_3 evaporates well, and the efficiency of the nanopowder production amounts to 23 g h^{-1}.**

Keywords: *laser ablation of fine-grained transparent materials, Helmholtz equation, laser radiation scattering, optical resonance, ytterbium fibre laser, nanoparticles.*

1. Introduction

The study of the processes accompanying ablation of targets made of a transparent porous dielectric is important for modelling and technology improvement of laser cutting, nanopowder production, and development of 3D technologies using such materials. In such studies, the following questions arise that seem to be important. What are the reasons for different ablation of materials having close thermal physical properties and transparency? Why are ablation threshold powers in porous transparent materials, as a rule, by an order of magnitude lower than in single crystals? What are the effects giving rise to ablation in these materials?

These questions arise as well for Nd:Y_2O_3, Nd:YAG, ZrO_2, Y_2O_3 (YSZ) or Al_2O_3 exposed to laser radiation with a wavelength lying in the transparency region of these materials. In the single-crystalline form they possess a general property of a small absorption index (10^{-3}–10^{-4} cm^{-1}) at λ = 1.07 μm [1–3] and, correspondingly, a sufficiently high threshold of optical breakdown. In particular, the surface damage threshold for single crystals of ruby or sapphire at the wavelength λ = 0.69 μm that corresponds to their transparency region amounts to 1–10 MW cm^{-2} for the pulse duration τ = 10–400 μs [4]. In the case of perfect optical quality, the breakdown threshold intensity for these single crystals is even higher [5]. Under these conditions, the destruction is achieved at the expense of the laser radiation absorption by structure microdefects or impurities. However, the targets of poorly sintered microparticles of Al_2O_3, Nd:Y_2O_3, or YSZ with the porosity ~50% are well evaporated even at much lower radiation intensity (0.46 MW cm^{-2}) with λ = 1.07 μm and τ = 50–4000 μs [6–10].

Earlier we proposed a model of the initial phase of ablation (before the formation of a laser torch) of a semitransparent melted layer that appears at the surface of a porous target made of yttrium oxide in the process of nanopowder production [6, 7]. In the model, we considered the absorption of the fibre laser radiation by some structure defects contained in the target that have a higher absorption index than the surrounding substance. It allowed a qualitative explanation of the multiple increase in the delay time in the formation of a laser torch in the case of evaporating a semitransparent target, as compared to the similar quantity for the pressed target, by the fact that the semitransparent target contained fewer defects. However, in the model the actually present processes of scattering and interference of laser radiation on the absorbing defects or other optical inhomogeneities of the target were not considered.

The necessity of considering these processes was demonstrated in a number of papers by the example of the interaction of laser radiation with a single particle. The authors of Refs [11, 12] have shown that at some combination of the incident light wavelength, the refractive index and the diameter of the particle, it can act as a high-Q resonator. In this case, the amplitudes of spherical modes of the scattered electromagnetic field, the eigenfrequency of which coincides with the frequency of the incident light, resonancely increases. This can lead to the growth of light intensity inside the particle by

V.V. Osipov, V.V. Platonov, E.V. Tikhonov Institute of Electrophysics, Ural Division, Russian Academy of Sciences, ul. Amundsena 106, 620016 Ekaterinburg, Russia;
e-mail: osipov@iep.uran.ru, platonov@iep.uran.ru;
V.V. Lisenkov Institute of Electrophysics, Ural Division, Russian Academy of Sciences, ul. Amundsena 106, 620016 Ekaterinburg, Russia; Ural Federal University named after the First President of Russia B.N. Yeltsin, ul. Mira 19, 620002 Ekaterinburg, Russia;
e-mail: lisenkov@iep.uran.ru

Received 7 December 2017
Kvantovaya Elektronika **48** (3) 235–243 (2018)
Translated by V.L. Derbov

two orders of magnitude and to the appearance of the Fano resonance in the interference of these resonance modes outside the particle with the light scattered by its surface. This results in the modulation of both the scattering angle and the total intensity of scattered radiation. Similar processes occur in the case of photon jet formation, i.e., an increase in light intensity in a narrow region located in the near diffraction zone of the transparent microparticle illuminated by laser radiation [13]. Such calculations were performed also in the study of photonic crystals [14]. We should note that the theoretical studies [11–14] are restricted to the clarification of the radiation intensity distribution inside or outside a single particle or an ensemble of particles, and the influence of the scattering factor on the radiation absorption by microparticles, their subsequent heating, and evaporation are not considered.

In the theoretical studies of the force effect of laser radiation with a sufficiently high mean power on powders or porous optical media, the latter are presented as a continuum with the mean characteristics. Work [15] considering the heating and melting of the SiO_2 ceramics with the porosity 50% by laser radiation with the intensity 10^2–10^5 W cm^{-2} can serve as an example. Gusarov [16] simulated the penetration of laser radiation into a homogeneous layer of powder of nontransparent mirror-reflecting metal particles, characterised by a certain effective scattering coefficient. These studies do not consider diffraction and interference effects that may arise in such media at a microscopic level. The only exception known to us is Ref. [17], where the transmission of laser radiation through the powder medium consisting of spherical metal particles with the diameter 1–12 μm was studied experimentally and theoretically. According to the developed 2D numerical model based on the Helmholtz equation, the light scattering by the particles leads to the formation of multiple local maxima of the radiation intensity between them. At the same time, the model does not consider the transparency of the particles, since it was developed for metal nontransparent microparticles.

The aim of the present paper is to propose a numerical model for the propagation of a laser beam with $\lambda = 1.07$ μm through the pressed powder of transparent microparticles (Al_2O_3, SiO_2, Y_2O_3, YSZ, CaF_2, MgF_2, BaF_2, etc.), based on the solution of Helmholtz wave equation, which would allow for refraction, reflection, and interference inside such a medium, as well as to check qualitatively its basic conclusions by the example of producing nanopowders of these materials using radiation of an ytterbium fibre laser.

2. Experimental

To prepare nanopowders of fluorite (CaF_2) and 1% Nd : Y_2O_3 we used an LS-07N ytterbium fibre laser and a repetitively pulsed CO_2 laser (LAERT). The construction and operation principle of the setup for preparing nanoparticles are thoroughly described in Refs [6, 7, 18]. In both cases, the target was installed in the evaporation chamber equipped with a focusing lens. The target evaporation was performed in the argon flow at atmospheric pressure, since at the temperatures above 900 °C the fluorite is hydrated by water vapours contained in the atmospheric air with the formation of gaseous HF [19]. The technical argon (purity 99.993 vol. %) was supplied from a standard vessel via a reductor. For the evaporation of fluorite by radiation of the fibre laser, the volume flow rate of argon amounted to 4.5 m^3 h^{-1}, and in the case of a CO_2 laser it was 5.3 m^3 h^{-1}. With the fibre laser, the nanopowder was obtained in the air pumped through the evaporation chamber by a membrane compressor. The air pressure in the chamber was equal to 1 atm, and the flow rate amounted to 4.5 m^3 h^{-1}. The nanoparticles, microdroplets and target fragments formed in the laser torch were transferred with the gas flow, first, into the cyclone for trapping micron-size particles and then into the bag filter, where the overwhelming majority of nanoparticles were precipitated. To provide uniform depletion of the target, it was moved by means of a mechanical drive.

The CO_2 laser irradiating the fluorite targets generated pulses with the duration ~330 μs and the energy 0.9 J (the peak power 7 kW). The mean power of radiation amounted to 450 W with the pulse repetition rate 500 Hz. The KCl lens with $F = 107$ mm focused the laser beam at the target into an elliptic spot with the size 0.75 × 0.9 mm. The peak radiation intensity amounted to 1.3 MW cm^{-2}. The linear velocity of laser beam motion relative to the target was equal to 35 cm s^{-1}.

The continuous-wave radiation of the ytterbium fibre laser was focused at the target surface by a silica lens with $F =$ 400 mm into a spherical spot with the diameter 430 μm. The laser radiation intensity averaged over the spot area was equal to 0.4 MW cm^{-2}. The velocity of beam scanning over the target surface amounted to 67 cm s^{-1}. Additional experiments with the evaporation of immobile fluorite target by single rectangular pulses having the power 600 W and the duration from 100 μs to 10 ms were carried out. In these experiments, the radiation was focused by lenses with the focal length 200, 400 or 600 mm. The focal spot diameters for the two latter lenses were 250 and 700 μm, and the light intensity in the spots was 1.2 and 0.16 MW cm^{-2}, respectively. After each laser pulse the target was moved.

The fluorite targets were made of nanopowder with the content of the base substance 98.6% (quality grade 'Pure'). The powder was compressed with a single-axis press into cylinders with the diameter 65 mm, which were sintered in the air in a chamber furnace during four hours. To avoid the pyrohydrolysis of CaF_2 in the target, its sintering temperature was chosen to be 740 °C, which is much lower than the temperature at which this process begins (900 °C). After the sintering, the relative density of the target amounted to ~60% of the theoretical one. The targets of 1% Nd : Y_2O_3 were prepared from the mechanical mixture of micropowders of simple oxides Y_2O_3 and Nd_2O_3 in a similar way. Their relative density after sintering at the temperature 1300 °C amounted to ~55%.

3. Theoretical model

The effect of fibre laser radiation on a transparent powder dielectric medium was studied by solving numerically the Helmholtz wave equation, which describes the propagation of an electromagnetic wave through the 2D medium, comprised by transparent particles with the refractive index n_p and air with $n_{air} = 1$:

$$\Delta E + k^2 \varepsilon_r E = 0,$$

where E is the amplitude of the electric field strength; $k = 2\pi/\lambda$ is the wavenumber; and ε_r is the dielectric constant of the material.

As a material to be studied, we have chosen MgF_2 ($n_p =$ 1.38), CaF_2 (1.43), BaF_2 (1.47), SiO_2 (1.54), BeO (1.71),

$MgAl_2O_4$ (1.70), Al_2O_3 (1.75), Y_2O_3 (1.90), and YSZ (2.12). Their absorption indices at $\lambda = 1.07$ μm have sufficiently small values (10^{-2}–10^{-4} cm^{-1}), i.e., the characteristic depth of radiation penetration into ideal single crystals of these materials amounts to 10^2–10^{-4} cm. Therefore, for the size of particles in the pressed target ~1 μm and the dimension of the calculation domain ~200 μm the intrinsic absorption plays no role in the general picture of scattering. Moreover, at the present stage of calculations we do not consider the heating of particles by laser radiation and, therefore, the temperature dependence of the refractive index n_p.

As a boundary condition of the problem, we used the condition of tangential electric field continuity at the boundary between two media with different refractive indices

$$\boldsymbol{n} \times \boldsymbol{E} = \boldsymbol{n} \times \boldsymbol{E}_0,$$

where $\boldsymbol{E}_0$ and $\boldsymbol{E}$ are the electric field strength vectors before and after the interface between the media, respectively; and $\boldsymbol{n}$ is the unit vector normal to the boundary. It was assumed that the boundaries of the calculation domain do not reflect radiation and are completely transparent.

The relation between the electric field strength amplitude $E(x, y)$ and the laser radiation intensity was expressed by the known formula for linearly polarised radiation [20] that in the SI units has the form:

$$E = \sqrt{\frac{2I}{c\varepsilon_0}},$$

where I is the intensity of laser radiation; c is the velocity of light in vacuum; and ε_0 is the electric constant.

In all calculations the intensity of the incident radiation I_0 was the same and amounted to 0.46 MW cm^{-2}, since this particular value was used in the experiment with the radiation focused by the lens with the focal length 400 mm into a spot with the diameter 430 μm. According to the above formula, this intensity corresponds to the electric field strength $E_0 = 1.81 \times 10^6$ V m^{-1}. The variable parameters were the refractive index of the particle material, n_p, and the particle diameter D. All calculations were performed for the radiation of the ytterbium fibre laser with $\lambda = 1.07$ μm.

In the calculations, we used two configurations of the calculation domain. Figure 1 presents the central part of the calculation domain used to model the interaction of radiation with a single spherical particle having the diameter D and the refractive index n_p, surrounded by the air with $n_{air} = 1$. The particle was placed in the rectangular calculation domain with the size 50 μm × 100 μm. This configuration of the calculation domain was mainly used to test the model. Moreover, some observed regularities are clearer in this case, since the field configuration is not affected by the scattering of radiation by the neighbouring particles. This simplifies the analysis of the results for powder media.

For numerical calculations of scattering of laser radiation by pressed powder, we used the model with the calculation domain geometry, qualitatively analogous to real targets used in nanopowder preparation experiments (Fig. 1b) In this case the rectangular domain with the size 24 μm × 200 μm was filled with spherical particles having the same refractive index n_p. To justify the choice of the mean particle size the initial powder of Y_2O_3 was photographed by means of the OLYMPUS BX51TRF-5 optical microscope. The size distribution of particles obtained by using the photographs [Fig. 1c, curve (*2*)] has shown that the diameters of the majority of particles in the initial micropowder amount to 400 nm–5 μm; however, there were individual particles with the diameter up to 8 μm. According to these considerations, the calculation domain was randomly filled with the particles having the diameters from 0.55 to 4.6 μm [Fig. 1c, curve (*1*)]. The determined distributions have normal-logarithmic form, their maxima virtually coinciding and corresponding to the diameter of the particles 1.5–1.7 μm. The packing density of particles in the calculation domain amounted to 55%, which corresponds to the relative density of the targets used in the experiments. It is necessary to note that the present model only qualitatively describes the real target of pressed micropowders, since in real powders and pressed compacts the particles have the shape of irregular polyhedrons rather than spheres.

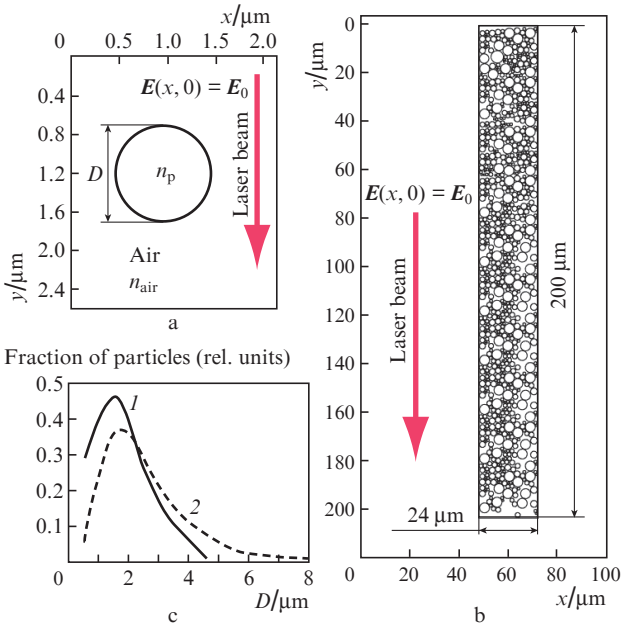

Figure 1. Calculation domain geometry for the cases of a single particle (a) and pressed powder (b), as well as the size distribution (c) of the particles in the calculation domain (*1*) and the particles of the initial raw material Y_2O_3 (*2*).

At the upper boundary of both calculation domains the value of the electric field strength amplitude was specified as $E_0 = 1.81 \times 10^6$ V m^{-1}. The radiation inside the calculation domain propagated in the direction shown by arrows in Fig. 1.

4. Discussion of calculated and experimental results

At the first stage, we solved the problem of scattering of the fibre laser radiation by individual particles. Figure 2 shows the intensity distributions for the fibre laser radiation scattered by particles of CaF_2 (Fig. 2a) and Y_2O_3 (Fig. 2b) with $D = 10$ μm. For clarity, the magnified central part of the calculation domain, containing a particle, is shown separately. In both cases, we should note that in some local areas of the calculation domain the intensity of the scattered radiation considerably exceeds the intensity of radiation incident on the particle. These areas of increased intensity will be conventionally referred to as regions of local maxima. Their origin is due

to the interference of two components of the laser radiation interacting with the particle. One of them is due to the radiation scattering by the outer surface of the particle. The other one is due to the refraction of radiation and multiple reflections inside the particle. In Fig. 2, with the change in the refractive index, one can observe the change in both the spatial localisation of the high-intensity region and the magnitude of the maximal intensity in this region. Thus, for CaF_2 ($n_p = 1.43$) the local maximum region is shaped as a 'tail' with the length $\sim 10\lambda$, resembling a photonic jet [13], in which the maximal intensity I_{max} amounts to 5.37×10^6 W cm^{-2}. When the refractive index is increased to 1.90 (Y_2O_3), the local maximum region practically does not expand beyond the particle. The radiation is focused either inside the particle, or very closely to its surface. The region of the local maximum already has not the shape of a jet. The length of it amounts to $\sim 2\lambda$, and the maximal intensity to $I_{max} = 1.04 \times 10^7$ W cm^{-2}, which is almost by two times greater than in the case of fluorite (CaF_2).

Thus, in the case of radiation scattering by transparent microparticles under a certain relation between the radiation wavelength, the particle diameter and the particle refractive index, the optical resonances can arise, capable of essential modification of the spatial distribution of the scattered radiation intensity. The intensity excess above the threshold value in the local maxima can significantly increase the probability of optical breakdown development inside the microparticle or at its surface (generally, in the powder medium). Hence, we calculated the dependence of the maximal radiation intensity with $\lambda = 1.07$ μm in the local maxima on the diameter of one scattering particle (by the example of Y_2O_3). As seen from Fig. 2c, this dependence is nonmonotonic. At the particle diameter $\lambda/5$ ($\sim$200 nm) the radiation is scattered by the particle surface according to the Rayleigh theory and does not penetrate into the particle. As the particle diameter grows, the maximal intensity in the local maxima also grows almost linearly. At the particle diameter greater than $\lambda/4$ ($\sim$270 nm), there is a noticeable penetration of the electromagnetic field into the particles. For the diameters 240–400 nm, the maximal intensity of laser radiation inside the particle amounts to $\sim 10^6$ W cm^{-2}. With a further increase in the particle diameter ($D > 3\lambda/4$), the dependence becomes sharply resonant. Thus,

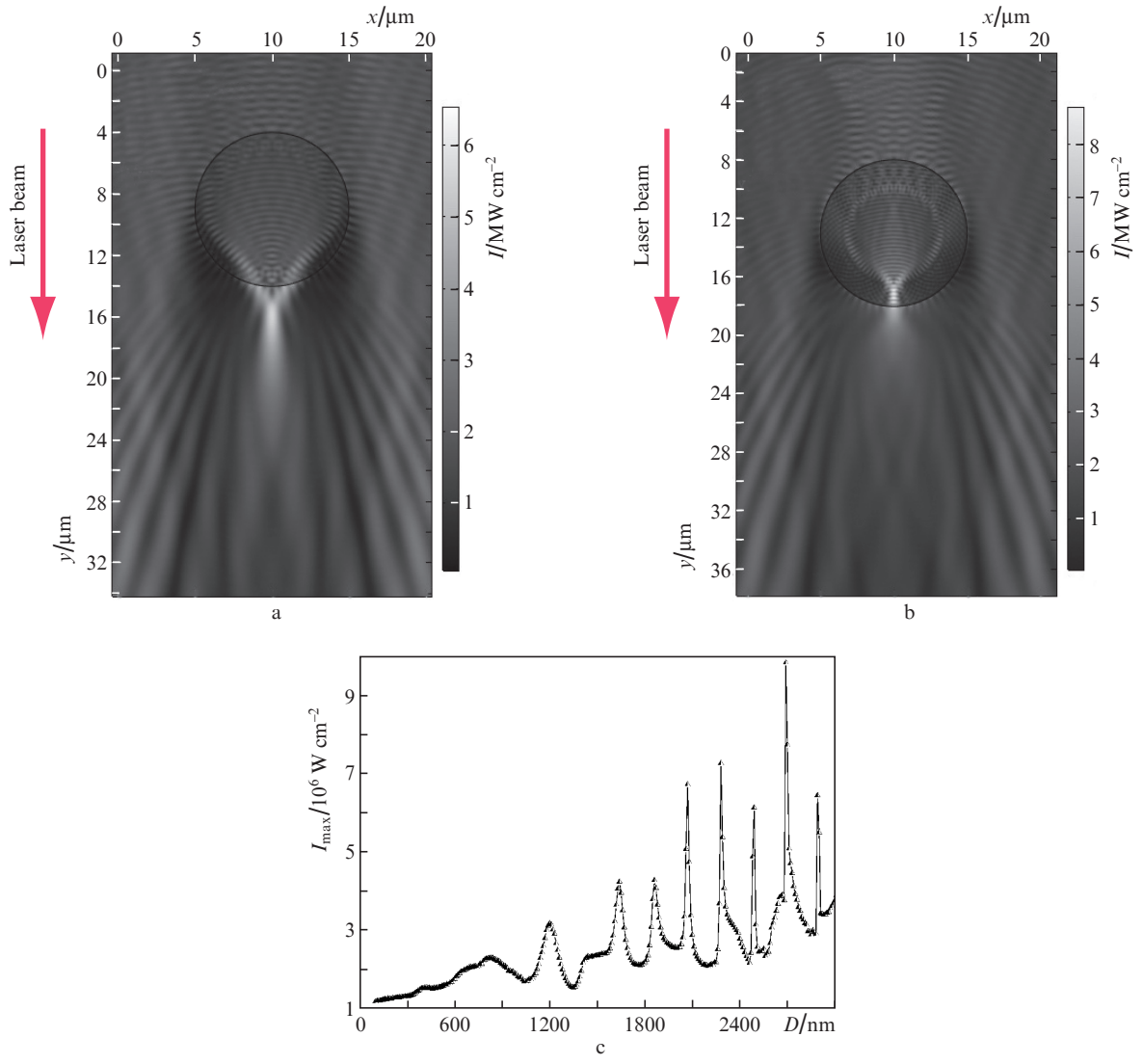

Figure 2. Distribution of the intensity of fibre laser radiation ($\lambda = 1.07$ μm, $I_0 = 0.46$ MW cm^{-2}) scattered by single particles of CaF_2 ($n_p = 1.43$) (a) and Y_2O_3 ($n_p = 1.90$) (b), as well as the dependence of the maximal intensity of scattered radiation I_{max} on the diameter D of the Y_2O_3 particle (c).

for a Y_2O_3 particle with the diameter 2690 nm the local maximum intensity achieves $\sim 10^7$ W cm^{-2}, which is nearly by 20 times higher than the intensity of laser radiation incident on the particle. Thus, at a certain relation between n_p, D, and λ, the transparent microparticle can behave as an optical resonator. In this case, the interference of the incident radiation with the radiation scattered and refracted by the particle surface, as well as that re-reflected inside the particle, leads to a resonance increase in the radiation intensity in some regions of the calculation domain. Both the spatial structure and the maximal value of intensity can essentially differ depending on the quantities n_p, D, and λ.

Real powder media, including the pressed targets used by us for evaporation, consist of multiple particles having different sizes. On the one hand, in such a medium a particle, for which the condition of the optical resonance is satisfied, will always exist. On the other hand, it is not reasonable to consider the local intensity maxima of individual particles, since it is the entire ensemble of particles comprising the target, which forms the scattered radiation pattern. In this connection, at the second stage of calculations we considered the interaction of laser radiation with the powder medium, consisting of spherical particles with the refractive index n (the geometry of the calculation domain is shown in Fig. 1b). Figure 3 presents the radiation intensity distributions in the powder medium of CaF_2 and Y_2O_3 for the area of the calculation domain, initially exposed to the radiation of the fibre laser (λ = 1.07 μm). One can see that the radiation scattering by the powder medium is chaotic due to the random positions of the particles. Obviously, in the case when the arrangement and size of the particles is essentially changed, the distribution of laser radiation in the powder will also change. Since the diameter of the majority of particles is in the range $(1-3)\lambda$, the laser radiation easily penetrates into them. Generally, a more complicated interference pattern of the laser beam attenuation due to refraction and scattering is observed, as compared to a single particle. However, in some local regions of the calculation domain the radiation intensity exceeds the intensity I_0 of radiation incident on the target because of concentration. It is essential that the radiation is scattered not only forward, but in the side and backward directions (by the adjacent or deeper localised microparticles). With the growth of the refractive index of the particles, the refraction and reflection of the laser beam at the boundaries are enhanced, which leads to an increase in the radiation intensity in the regions of maxima located near the target surface.

For better understanding of the intensity variations of the leaser radiation propagating through the powder we divided the calculation domain into layers, perpendicular to the propagation direction of the incident laser beam. The averaging of the scattered radiation intensity in each layer allowed the numerical characterisation of the radiation intensity attenuation in the course of propagation through the target. Figure 4 presents the dependences obtained for CaF_2, Al_2O_3, Y_2O_3, and YSZ. It is seen that the radiation intensity strongly fluctuates over the entire depth of penetration; however, it gener-

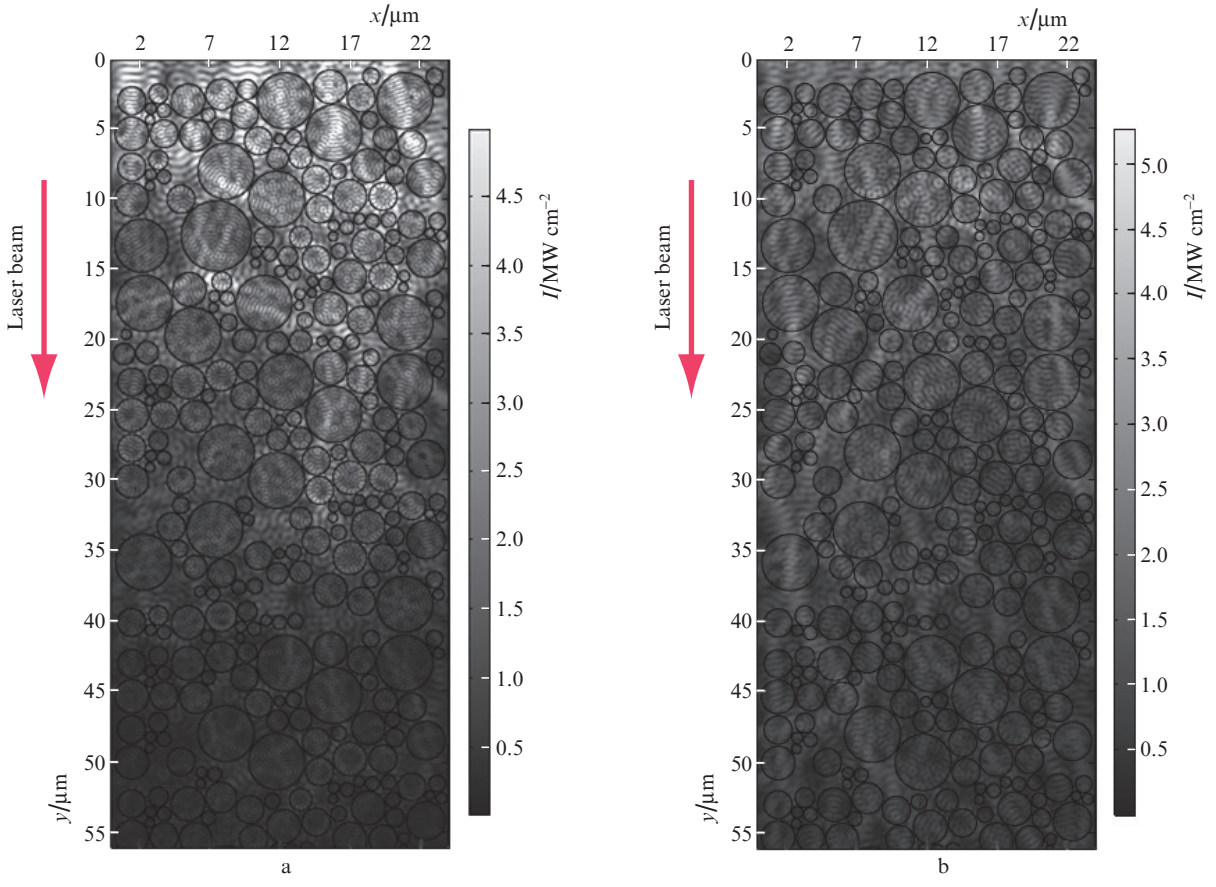

Figure 3. Intensity distributions of the fibre laser radiation with I_0 = 0.46 MW cm^{-2}, scattered in the pressed powders of CaF_2 (n_p = 1.43) (a) and Y_2O_3 (n_p = 1.90) (b).

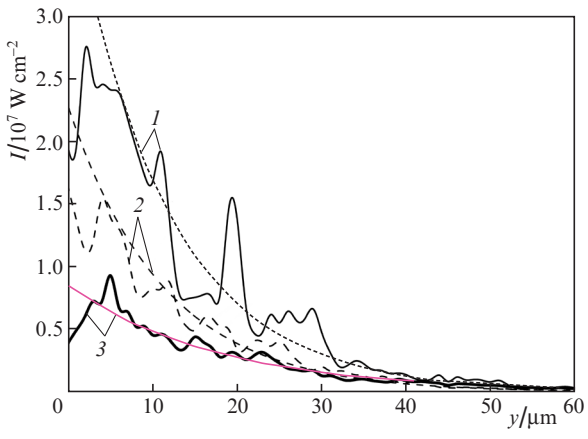

Figure 4. Depth distributions of the scattered radiation intensity, averaged over the layers of the calculation domain, for the powders of YSZ (*1*), Al_2O_3 (*2*), and CaF_2 (*3*), and their approximations by the Bouguer law (λ = 1.07 μm, I_0 = 0.46 MW cm^{-2}).

ally decreases with increasing depth. The decrease could be quantitatively estimated by approximating the processed data by the Bouguer law $I = I_0\exp(-\alpha y)$, where α (cm^{-1}) is the effective attenuation index, depending only on the scattering of radiation by particles.

The processing of the calculated data using the above method allowed the numerical estimate of the characteristic depth y_α of the radiation attenuation in pressed powders of all materials under study. Figure 5 shows the dependence of this parameter on the refractive index of the particle material for the wavelength of the incident radiation 1.07 μm (solid curve). With the growth of the refractive index n_p of the particle material from 1.38 (MgF_2) to 2.12 (YSZ), the characteristic depth of attenuation of the laser beam in the medium decreases from 19 to 11 μm due to stronger scattering. An almost sharp fall is observed in the range of refractive index values n_p = 1.38–1.75. Therefore, for the fluorite powder (CaF_2) the parameter y_α = 17 μm, which is by 1.5 times greater than for the yttrium oxide.

On the other hand, the optical breakdown in a powder medium is first expected to arise at the positions where the intensity of the scattered radiation exceeds the threshold

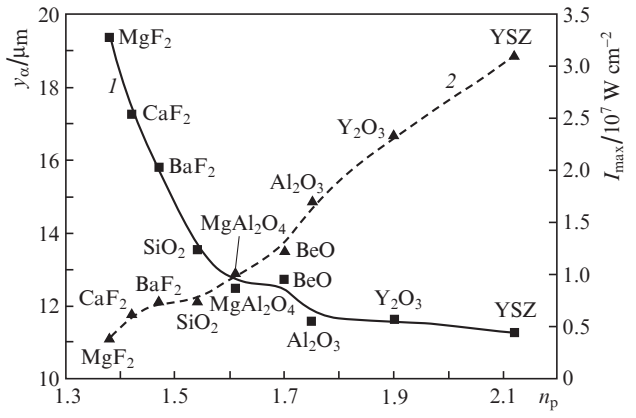

Figure 5. Dependences of the characteristic depth of laser radiation attenuation y_α (*1*) and the maximal radiation intensity in the region of the strongest local maximum I_{max} (*2*) on the refractive index n_p for the particles made of different materials (I_0 = 0.46 MW cm^{-2}).

value. Therefore, it is important to study the local maxima of intensity arising in the process of scattering rather than the laser radiation intensity averaged over horizontal layers. Figure 5 presents the dependence of the maximal intensity of radiation achieved in the strongest local maximum in the calculation domain on the refractive index of the material of particles. As n_p decreases from 2.12 (YSZ) to 1.38 (MgF_2), the intensity in the strongest local maximum of the calculation domain is seen to decrease from ~31 MW cm^{-2} (YSZ) to ~4.8 MW cm^{-2} (MgF_2). For fluorite and yttrium oxide, I_{max} amounts to ~6 and ~23 MW cm^{-2}, respectively.

Thus, the scattering of the radiation of the ytterbium fibre laser in the targets made of powders of these materials leads to the fact that, depending on the particles refractive index, in some local regions of the target the radiation intensity can exceed the intensity of the incident radiation by 10–67 times! If this happens in the volume or at the surface of a certain particle, the concentration of laser radiation must cause its optical destruction. We believe that in these local maxima the initial heating of the target begins. Then the dynamics of heating can develop according to the model [6, 7], in which because of the nonlinear dependence of the absorption index on temperature a positive feedback arises between the absorption of radiation and the temperature of material of the particles. As a result, the target material experiences fast heating in the region of the focal spot of the laser beam, followed by melting and evaporation. If the radiation intensity in such local maxima appears to be smaller than the threshold value, with the thermal conductivity heat losses taken into account, the heating of the appropriate regions of the target will be insufficient to initiate laser ablation.

The results of our calculations show that the refractive index of the particle material is one of the most important factors affecting the possibility of laser ablation of densely packed powders. Although for YSZ and MgF_2 the values of this parameter differ only by 1.6 times, the maximal levels of the radiation intensity values, locally achieved in particular positions within the pressed powders, differ already by 6.4 times (Fig. 5).

All these facts are important not only from the fundamental point of view, but also in practically significant applications, when it appears to be necessary to use a continuous-wave ytterbium fibre laser or a Nd:YAG laser having a moderate or small power in different technologies of processing transparent highly porous dielectrics. In this case, the intensity of radiation incident on the target, as a rule, appears to be relatively small (~1 MW cm^{-2} and smaller), i.e., is below the threshold of optical damage of a material free of pores and other optical inhomogeneities. These conditions are implemented in the process of producing nanopowders of transparent oxides YSZ, Nd:Y_2O_3, or Nd:YAG by evaporating the target sintered from a micropowder and having the porosity ~50%, by means of a cw fibre laser with the power 0.6–1 kW [6–8]. In this connection, we studied the preparation of CaF_2 nanopowder (n_p = 1.43) using the LS-07N fibre laser. The obtained data were compared with the results of an analogous experiment for 1% Nd:Y_2O_3, having a much greater refractive index (n_p = 1.91) [21]. It is necessary to emphasise that single crystals of these materials at λ = 1 μm have very low absorption coefficients (3×10^{-3} cm^{-1} for 1% Nd:Y_2O_3 and 2×10^{-4} cm^{-1} for CaF_2) [3, 22].

The target of a pressed and poorly sintered powder of 1% Nd:Y_2O_3 is evaporated well enough at the cw radiation power 600 W and the intensity at the target surface (I_0 =

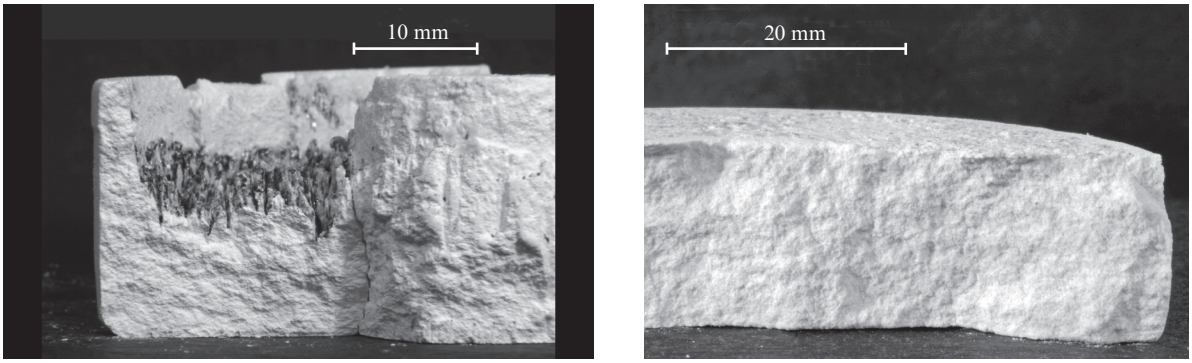

a b

Figure 6. Photograph of the fracture of the targets of 1% $Nd:Y_2O_3$ (a) and CaF_2 (b) after the impact of the cw radiation of the fibre laser with the power 600 W and the intensity $I = 0.4$ MW cm^{-2}.

0.4 MW cm^{-2}), lower than the optical damage threshold for single crystals of this composition. The target surface becomes very rough and coated with a layer of a transparent melt (Fig. 6a). When the laser radiation propagates through this pressed target, the radiation concentrates in some locations up to a sufficiently high intensity I_{max}, the value of which, according to our calculation, can be as large as 23 MW cm^{-2}, which exceeds the optical damage threshold. The efficiency of producing the nanopowder by ablation under these conditions amounted to 23 g h^{-1}. The produced nanoparticles are spherical (see Fig. 7a), and their mean size is 13.6 nm.

In turn, under the action of cw radiation of the ytterbium fibre laser with the power 600 W and intensities 0.4, 1.2 and 0.16 MW cm^{-2}, no evaporation of the CaF_2 target occurred, and no laser torch appeared at its surface. After 10 minutes of exposure to radiation, practically no signs of laser ablation could be seen at the target surface (Fig. 6b). The target was not coated with a melted layer, which is always formed under multiple evaporation of the material by radiation having a high mean power. One can see only weak traces of the target surface heating by laser radiation. At the wall of the evaporation chamber, in the bag filter, and in the cyclone no products of ablation (nanopowder, fragments of target, droplets) ever appeared. We should note that in the nanopowder production under our conditions the laser beam is scanned over the target with the velocity 67 cm s^{-1}, i.e., the time of displacement over a beam spot size amounts to 370–1000 μs. During this interval, the material at the given position of the target can merely have no time to be heated and melted. To eliminate this factor, we performed several experiments, in which single rectangular pulses or radiation with the duration 100 μs–10 ms, power 600 W, and intensity 0.16– 1.2 MW cm^{-2} affected the immobile target of CaF_2. After the impact of pulses shorter than 10 ms, no visible changes on the surface of the target were observed. In our opinion, the refractive index of fluorite is too small, and the intensity of the scattered radiation inside

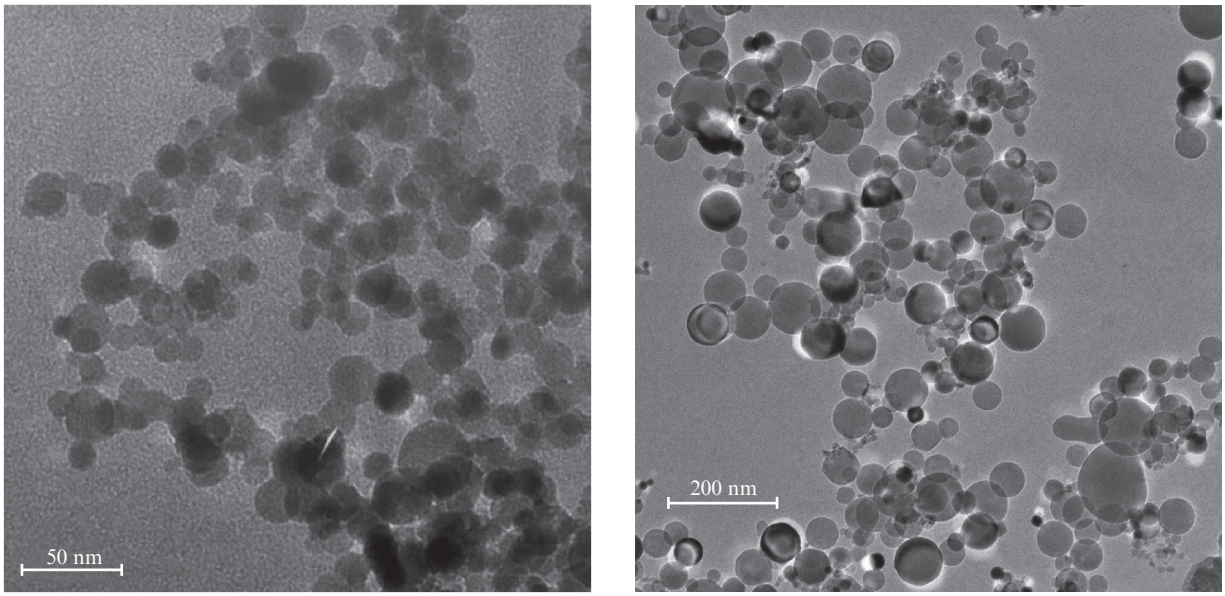

a b

Figure 7. Photographs of nanoparticles of 1% $Nd:Y_2O_3$, synthesised by means of the fibre ytterbium laser (a) and CaF_2 nanoparticles produced using the CO_2 laser (b).

the target does not achieve the value necessary for fast melting and evaporation of the material even at the local maxima. In this case, the radiation of the fibre laser is completely scattered in the target volume and heats it as a whole.

If the target material of pressed powder has low transparency or is not transparent at all at the laser wavelength, then its optical damage threshold will be significantly lower than that for transparent materials. In this case, the laser radiation will be absorbed at much smaller depth, and the factor of radiation scattering in such medium will play no key role in its ablation. In particular, at the wavelength of the CO_2 laser the single crystal of CaF_2 is half-transparent, and its absorption index equals 7.2 cm^{-1} [23]. This is by four orders of magnitude higher than for the radiation of the fibre laser. For this reason the target made of the micropowder of CaF_2 and having the porosity 61% in our experiments was evaporated well by means of the radiation of the repetitively pulsed CO_2 laser with the mean power 450 W and peak intensity 1.3 MW cm^{-2} at the target. In this case, the efficiency of fluorite nanopowder production amounted to 14.8 g h^{-1}. Figure 7b presents a photograph of the produced nanoparticles obtained by a JEM JEOL 2100 transmission electron microscope. It is seen that the nanoparticles are almost spherical, and the arithmetic mean diameter equals 39 nm. From the data of X-ray phase analysis, 96 mass % of the nanopowder has the phase of fluorite (Fm-3M, a = 5.468 Å), and the rest part has the tetragonal phase (P4/mmm, a = 3.74 Å, c = 2.68 Å).

Thus, the results of our experiments qualitatively correspond to the regularities and trends revealed in the modelling of propagation of fibre laser radiation through densely packed transparent microparticles. Data that are more precise can be obtained by completing the model with the heat conduction equation, allowing for the temperature dependence of the absorption index of the material. It will be possible to compare the results of these calculations with the delays of the laser torch appearance under irradiation of targets of pressed microparticles with different refractive indices, which is supposed to be done in future.

5. Conclusions

In the present paper the effect of high-power fibre laser radiation with λ = 1.07 μm on densely packed powders of transparent oxides and fluorides with small indices of intrinsic absorption (10^{-2}–10^{-4} cm^{-1}) and different refractive indices (n_p = 1.38–2.12) is studied theoretically and experimentally.

A 2D model of the impact of laser radiation on the pressed powder of transparent dielectric is elaborated. For this purpose, the Helmholtz equation was solved numerically, which allowed direct description of refraction, re-reflection, and interference of the laser radiation inside the medium. The modelling was performed for single and densely packed spherical microparticles of different diameters (0.5–4.6 μm). The following properties were demonstrated.

1. The laser radiation scattering on a single particle or in a powder in some local spatial regions yields the intensity exceeding the intensity of the incident radiation by many times. The formation of these local intensity maxima is related to the interference of the incident radiation, reflected from the surface of the particles, with the radiation that penetrates through the particle surface and is refracted and multiply reflected inside. In the case of a single particle with the diameter greater than $3\lambda/4$, the intensity of radiation in such local maxima resonancely depends on the particle diameter and can vary by a few times. In the powder containing microparticles of different sizes, the distribution of the scattered radiation intensity becomes much more chaotic.

2. A greater refractive index of the particle material increases the intensity in the local maxima both in a single particle and in a powder. On the contrary, the characteristic attenuation depth of the laser radiation in the powder decreases due to the scattering. In particular, for the scattering of radiation with the initial intensity I_0 = 0.46 MW cm^{-2} in the powder of CaF_2 (n_p = 1.43) the radiation intensity in the strongest local maximum I_{max} amounts to 6 MW cm^{-2}. For the powder of Y_2O_3 having a greater refractive index (n_p = 1.90) the maximal intensity increases to ~23 MW cm^{-2}.

3. The concentration of the scattered laser radiation in some local regions of pressed targets can lead to intensities essentially exceeding the threshold of the medium optical breakdown, even when the intensity of the incident radiation is below the threshold. The possibility of ablation occurrence in this case is directly related to the value of the refractive index of the particles, since with its increase the intensity of radiation in local maxima also increases.

The results of numerical calculations are qualitatively confirmed by the experimental data. Indeed, under the conditions approximately corresponding to the calculations (λ = 1.07 μm, I_0 = 0.16–1.2 MW cm^{-2}, D = 0.4–8 mm, the target porosity 55%–60%) the target ablation was absent. In this case the scattered radiation intensity in the region of each local maximum inside this target was below the ablation threshold, while for the target made of 1% $Nd:Y_2O_3$ having a greater refraction index (n_p = 1.91) the stable ablation was observed and the efficiency of the nanopowder production approached 23 g h^{-1}.

Acknowledgements. The present work was performed within the frameworks of the State Research Task No. 0389-2014-0027. It was also partially supported by the Russian Foundation for Basic research (Grant No. 17-08-00064 A).

References

1. Belov N.N. *Kristallografiya*, **34** (5), 1185 (1989).
2. Innocenzi M.E., Swimm R.T., Bass M., French R.H., Kokta M.R. *J. Appl. Phys*., **68**, 1200 (1990).
3. Hideyasu Tsuiki, Toshiaki Masumoto, Koichi Kitazawa, Kazuo Fueki. *Jpn J. Appl. Phys*., **21** (7), 1017 (1982).
4. Danileiko Yu.K., Manenkov A.A., Prokhorov A.M., Khaimov-Mal'kov V.Ya. *Sov. Phys. JETP*, **31** (1), 18 (1970) [*Zh. Eksp. Teor. Fiz*., **58** (1), 31 (1970)].
5. Danileiko Yu.K., Manenkov A.A., Nechitaylo V.S. *Trudy FIAN*, **101**, 31 (1978).
6. Osipov V.V., Lisenkov V.V., Platonov V.V. *Appl. Phys. A*, **118**, 1133 (2015).
7. Osipov V.V., Lisenkov V.V., Platonov V.V., Orlov A.N., Podkin A.V., Savvin I.A. *Tech. Phys*., **59** (5), 716, 724 (2014) [*Zh. Tekh. Fiz*., **84** (5), 88, 97 (2014)].
8. Kotov Y.A., Samatov O.M., Ivanov M.G., Murzakaev A.M., Medvedev A.I., Timoshenkova O.R., Demina T.M., V'yukhina I.V. *Techn. Phys*., **56** (5), 652 (2011) [*Zh. Tekh. Fiz*., **81** (5), 65 (2011)].
9. Osipov V.V., Solomonov V.I., Spirina A.V., Lisenkov V.V., Platonov V.V., Podkin A.V. *Opt. Spectrosc*., **122** (1), 74 (2017) [*Opt. Spektrosk*., **122** (1), 169 (2017)].
10. Osipov V.V., Lisenkov V.V., Platonov V.V., Podkin A.V., Tikhonov E.V., Evtushenko G.S., Trigub M.V., Fedorov K.V. *Quantum Electron*., **46** (9), 821 (2016) [*Kvantovaya Elektron*., **46** (9), 821 (2016)].
11. Tribel'skii M.I. *J. Opt. Technol*., **84** (7), 431 (2017) [*Opt. Zh*., **84** (7), 4 (2017)].

12. Tribelsky Michael I., Miroshnichenko Andrey E. *Phys. Rev. A*, **93**, 053837 (2016).
13. Geints Yu.E., Zemlyanov A.A., Panina E.K. *Quantum Electron*., **41** (6), 520 (2011) [*Kvantovaya Elektron*., **41** (6), 520 (2011)].
14. Rybin M.V., Khanikaev A.B., Inoue M., Samusev K.B., Steel M.J., Yushin G., Limonov M.F. *Phys. Rev. Lett*., **103**, 023901 (2009).
15. Galaktionov A.V., Stepanov S.V. *High Temperature*, **28** (1), 105 (1990) [*Teplofiz. Vysok. Temp*., **28** (1), 124 (1990)].
16. Gusarov A.V. *Quantum Electron*., **40** (5), 451 (2010) [*Kvantovaya Elektron*., **40** (5), 451 (2010)].
17. Kharanzhevskii E.V., Kostenkov S.N. *Vestn. Udmurtskogo Univ., Ser. Fiz., Khim*., (3), 33 (2012).
18. Osipov V.V., Platonov V.V., Lisenkov V.V., in *Handbook of Nanoparticles* (Switzerland: Springer Intern. Publ., 2015) Vol. 2; DOI 10.1007/978-3-319-13188-7_8-1.
19. Rakov E.G., Teslenko V.V. *Pirogidroliz Neorganicheskikh Ftoridov* (Pyrohydrolysis of Inorganic Fluorides) (Moscow: Energoatomizdat, 1987) p. 46.
20. Karlov N.V. *Lektsii po kvantovoi elektronike* (Lectures on Quantum Electronics) (Moscow: Nauka, 1988) p. 30.
21. Osipov V.V., Orlov A.N., Kashirin V.I., Lisenkov V.V. *Instrum. Exp. Tech*., **56** (1), 80 (2013) [*Prib. Tekh. Eksp*., (1), 90 (2013)].
22. Palashov O.V., Khazanov E.A., Mukhin I.B., Smirnov A.N., Mironov I.A., Dukel'skii K.V., Garibin E.A., Fedorov P.P., Kuznetsov S.V., Osiko V.V., Basiev T.T., Gainutdinov R.V. *Quantum Electron*., **39** (10), 943 (2009) [*Kvantovaya Elektron*., **39** (10), 943 (2009)].
23. Grigoriev I.S., Meilikhov E.Z. *Handbook of Physical Quantities* (Boca Raton: CRC Press, 1996; Moscow: Energoatomizdat, 1991).